Equilibrium states and vortex domain wall nucleation in ferromagnetic nanotubes

P. Landeros,[1,*] O. J. Suarez,[1] A. Cuchillo,[1] and P. Vargas[1,2]

[1]*Departamento de Física, Universidad Técnica Federico Santa María, Avenida España 1680, Casilla 110-V, 2340000 Valparaíso, Chile*

[2]*Max-Planck-Institute for Solid State Research, Heisenbergstrasse 1, D-70569 Stuttgart, Germany*

We present a theory to describe the equilibrium states and nucleation phenomena in ferromagnetic tubular nanostructures. We show that, in a broad range of geometrical parameters, the magnetic state of a nanotube is a mixture of vortex states, at tube ends, and a uniform magnetization state along the tube axis. The incomplete vortex structures confined at the tube ends are growing domain walls which can be set in motion with external fields, current-driven techniques, or thermal assistance. We also show how the well-known nucleation problem can be better understood with basis in the theoretical model presented in this paper.

PACS number(s): 75.75.+a, 75.10.−b, 75.60.Jk, 75.60.Ch

I. INTRODUCTION

Since the progress to synthesize and characterize nanostructures, there is always the interest to evaluate the potential of one-dimensional nanostructures as functional components in device fabrication. In particular in the last few years, the fabrication of magnetic nanotubes of different materials (organic and inorganic) has triggered a new and broad research field, including their physical properties and its possible applications in different areas. Although the physical properties of ferromagnetic nanowires have been extensively investigated, magnetic nanotubes have been poorly explored so far in spite of some potential advantages over solid cylinders. Nanotubes exhibit a core-free magnetic configuration, which avoids a mathematical singularity in the tube axis, leading to a more controllable and faster reversal process, guaranteeing reproducibility and efficiency, and therefore a better manipulation of their rich magnetic properties. Ferromagnetic tubular structures are objects of current research not only for the understanding of their basic properties but also because they exhibit many potential applications in nanotechnology and biotechnology. Data storage, magnetic sensors, microelectronics, and magnetic imaging[1–5] as well as biomedical applications, such as cell separation, drug delivery, or biosensing,[6–8] are some examples of the multifunctionality of tubular magnetic structures, which due to their low density can float in solutions making them suitable for many applications in biotechnology.[6–8]

From the experimental point of view, there are several methods for the fabrication of magnetic tubes, which includes, for example, hydrogen reduction,[1] electrodeposition,[2,3] and atomic layer deposition[5] into porous membranes. From the theoretical side, the knowledge of basic magnetic properties, such as the internal magnetic structure or equilibrium states, magnetization reversal process, nucleation field, and coercivity, is of fundamental importance. Magnetic measurements,[5] numerical simulations,[4] and analytical calculations[9,10] on such tubes have identified two main equilibrium states: an in-plane magnetic ordering, namely, the flux-closure vortex state, and a uniform state with all the magnetic moments pointing parallel to the axis of the tube. Besides these two main states, micromagnetic simulations have demonstrated the existence of a "mixed"

(M) state, which is a mixture of the ferromagnetic (F) and vortex (V) states.[4,11,12] This new state (see Fig. 1) presents a uniform magnetization along the middle region of the tube and near the lower and upper surfaces the magnetization deviates from the uniformity in order of reduce stray or dipolar fields. The predominance of one of them depends upon the specific geometry of the nanotube and also on the material of which the nanotube was synthesized. Moreover, the existence of the mixed state is closely related with the phenomenology of nucleation and subsequent reversal process of the magnetization. Recently, it was shown that the size-dependent reversal process occurs via nucleation and propagation of domain walls, which can be a transverse wall for tube radius (R) smaller than a critical radius $[R_c(\beta)]$ or a vortex wall for $R > R_c(\beta)$.[13] This critical radius depends on the magnetic material[13] and on a shape factor, which is defined as $\beta \equiv R_i/R$, with R_i as the internal radius of the tube. This critical radius ranges from a few nanometers to 20 nm approximately, and therefore, since nanotubes experimentally fabricated have usually $R > R_c(\beta)$, we can expect that the nucleation and propagation of a vortex domain wall be the dominant magnetization reversal mechanism for magnetic nanotubes.[13] Thus, it is natural to think that in zero applied field, the deviation of the magnetization near the tube ends is most likely an incomplete vortex domain wall structure, as pointed out recently by Lee *et al.*,[11] as well as by Chen *et al.*[12] In this paper we present a theory to describe the actual magnetic equilibrium state in ferromagnetic nanotubes. Our model enables us to investigate the size-dependent equilibrium states as well as the nucleation field, that is, the value of the external field such that the magneti-
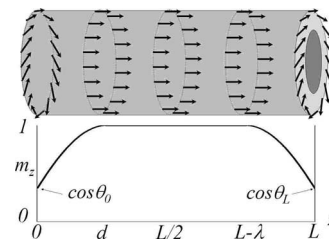

FIG. 1. Illustration of the mixed state in magnetic nanotubes. In the middle region the magnetization is uniform, whereas in the extremes we have incomplete vortex domains.

zation begin to deviate from the saturated state, which is a quantity closely related to the coercivity. Also we will reinforce our theoretical study with numerical simulations at the atomic level, based on the Monte Carlo method with scaling of the exchange constant.[14–17] We perform simulations on different geometries with the aim to reproduce the equilibrium states based on Monte Carlo simulations.

This paper is organized as follows. In Sec. II we describe our theoretical model, whereas in Sec. III we describe our numerical simulations. In Sec. IV we present the results and discussion comparing theory and simulations. Nucleation phenomena as well as magnetization reversal are also discussed here. Conclusions are summarized in Sec. V and mathematical details are presented in the Appendix.

II. THEORETICAL MODEL

Geometrically, tubes are characterized by their external and internal radii, R and R_i, respectively, and length L. It is convenient to define the ratio $\beta \equiv R_i/R$ so that $\beta = 0$ represents a solid cylinder and $\beta \rightarrow 1$ correspond to a very narrow tube. We adopt a simplified description of the system in which the discrete distribution of magnetic moments is replaced by a continuous one, defined by a function $\mathbf{M}(\mathbf{r})$ such that $\mathbf{M}(\mathbf{r})\delta v$ gives the total magnetic moment within the element of volume δv centered at $\mathbf{r}$. The total magnetic energy is composed of four contributions which are taken from the well-known continuum theory of ferromagnetism.[18] That is, $E = E_x + E_d + E_K + E_Z$, where $E_x = A \int \Sigma (\boldsymbol{\nabla} m_i)^2 dv$ is the exchange energy,[18] with $m_i = M_i/M_s$ ($i = x, y, z$) as the Cartesian components of the magnetization normalized to the saturation value M_s ($\mathbf{m} = \mathbf{M}/M_s$) and A as the stiffness constant. The dipolar contribution is written as $E_d = (\mu_0/2) \int \mathbf{M} \cdot \boldsymbol{\nabla} U dv$, with U as the magnetostatic potential,[18] whereas E_K is the magnetocrystalline anisotropy, which can be cubic (c) or uniaxial (u) depending on the sample. The last contribution is the Zeeman term $E_Z = -\mu_0 \int \mathbf{M} \cdot \mathbf{H} dv$, where $\mathbf{H}$ is an external field. We will proceed to describe the magnetization of the mixed state and evaluate the magnetic energy of the system.

A. Mixed state magnetization

The arrangement of magnetic moments in a tube can be seen as a uniform state in the middle region of the tube but with two deviations of the magnetization, such as an incomplete vortex walls localized at the tube ends (see Fig. 1). The magnetization field of such a magnetic configuration can be written in the following way:

$$\mathbf{m}(z) = m_z(z)\hat{\mathbf{z}} + m_\phi(z)\hat{\phi}, \qquad (1)$$

where

$$m_z(z) = \cos \Theta(z), \quad m_\phi(z) = \sin \Theta(z). \qquad (2)$$

We adopt a trial function for $\Theta(z)$ with four adjustable parameters, which is given by

$$\Theta(z) = \begin{cases} \theta_0(d-z)/d, & 0 \leq z \leq d \\ 0, & d \leq z \leq L - \lambda \\ \theta_L(z - L + \lambda)/\lambda, & L - \lambda \leq z \leq L, \end{cases} \qquad (3)$$

where d and λ (see Fig. 1) are the dimensions of the regions where the magnetization deviate from the z axis. θ_0 and θ_L correspond to angles of the magnetization with the z axis evaluated at the tube ends ($z = 0$ and $z = L$, respectively). For example, in the bottom surface of the tube ($z = 0$), $\Theta(0) = \theta_0$, and $m_z(0) = \cos \theta_0$, that is, the z component of the tube magnetization. With this form for the magnetization we can describe in detail the mixed state as a function of the tube geometry. Also we can obtain the full ferromagnetic order in the limit $m_z(0) = m_z(L) = 1$ ($\theta_0 = \theta_L = 0$) which occurs particularly for smaller dimensions. The set of model parameters $\{d, \lambda, \theta_0, \theta_L\}$ enables us to investigate in detail the magnetic properties of nanotubes whose geometrical parameters are R, β, and L. The model parameters are such that they minimize the total energy for each set of geometrical parameters. It is worth mentioning that the four-parameter variational problem can be simplified considerably if the tube is symmetric, that is, if there is no difference between both tube ends. Therefore, in some special cases, the four-parameter model is reduced to a two-parameter model $\{d, \theta_0\}$ when $d = \lambda$ and $\theta_0 = \theta_L$.

Another characteristic of our model is that we can investigate the nucleation of a vortex domain wall. Usually, and for simplicity, the nucleation field it is calculated in the so-called curling mode, assuming an infinite sample.[18–21] In the curling mode there is no dependence on the axial coordinate (z) and the first deviation of the magnetization occurs along the entire sample, not only in the tube ends, as expected. In our model we can obtain with precision the value of the external field at which the vortex wall nucleates. Thus the nucleation field is such that the angles $\theta_0 = \theta_L \gtrsim 0$. A detailed study of the nucleation field and coercivity will be published elsewhere.

B. Mixed state energy

If we know the magnetization vector $\mathbf{M}(\mathbf{r}) = M_s \mathbf{m}(\mathbf{r})$ [Eq. (1)] and the geometry of the ferromagnetic body, we can obtain the total energy, $E = E_x + E_d + E_K + E_Z$, of the magnetic nanotube in the mixed state, which is calculated in the continuum approach described above. After straightforward calculations (see the Appendix), the exchange energy (E_x) of the mixed state can be cast in the form

$$E_x = \pi A \ln(1/\beta) f_x + \pi A R^2 (1 - \beta^2) \left(\frac{\theta_0^2}{d} + \frac{\theta_L^2}{\lambda} \right), \qquad (4)$$

where

$$f_x \equiv d \left(1 - \frac{\sin(2\theta_0)}{2\theta_0} \right) + \lambda \left(1 - \frac{\sin(2\theta_L)}{2\theta_L} \right). \qquad (5)$$

The dipolar term E_d can be separated in surface and volumetric contributions, that is, $E_d = E_{ds} + E_{dv}$, and is given by (see the Appendix)

$$E_d = \frac{\pi\mu_0 M_s^2}{2}\int_0^\infty g^2(q)[q\Omega(q) - \Gamma(q)]dq, \qquad (6)$$

where $g(q) \equiv (R/q)[J_1(qR) - \beta J_1(qR\beta)]$ [here $J_1(x)$ are Bessel functions of first kind] and $\Omega(q)$ and $\Gamma(q)$ [Eqs. (A5) and (A7)] are related to the surface and volumetric contributions, respectively. Usually, the anisotropy contribution E_K can be cubic E_c or uniaxial E_u depending on sample preparation and magnetic material. The uniaxial anisotropy E_u can be written as

$$E_u = -K_u \pi R^2 (1 - \beta^2)(L - f_x/2), \qquad (7)$$

where K_u is the uniaxial anisotropy constant and f_x is given by Eq. (5). If the easy (hard) direction is the axis of the tube, then $K_u > 0$ ($K_u < 0$). Also, the cubic anisotropy E_c gives

$$E_c = \frac{\pi K_c}{256} R^2 (1 - \beta^2) f_c, \qquad (8)$$

where $f_c \equiv (44\theta_0 - 8\sin 2\theta_0 - 7\sin 4\theta_0)d/\theta_0 + (44\theta_L - 8\sin 2\theta_L - 7\sin 4\theta_L)\lambda/\theta_L$. Finally, the Zeeman energy can be expressed as

$$E_Z = -\pi\mu_0 M_s H R^2 (1 - \beta^2)$$
$$\times \left[L - d\left(1 - \frac{\sin\theta_0}{\theta_0}\right) - \lambda\left(1 - \frac{\sin\theta_L}{\theta_L}\right) \right]. \qquad (9)$$

With above expressions for the different energy contributions, we can investigate the magnetic equilibrium state diagram (or phase diagram) as well as describe nucleation phenomena. We remark that the total energy is further reduced if the nanotube is symmetric (when $d = \lambda$ and $\theta_0 = \theta_L$). In those cases we minimize the total energy only with regard to d and θ_0.

III. NUMERICAL SIMULATIONS

Let us consider for simplicity a hollow cylindrical structure which is characterized by two parameters, its radius R and its length L. According to these values the internal magnetic structure shows different behaviors. The scaling technique was developed by d'Albuquerque e Castro *et al.*[14] and was used to build a phase diagram showing the relative stability of three magnetic configurations as a function of the cylinder geometry. To build such a phase diagram, a smaller cylinder than that of the real system was used, in such a way that the treatment of much less atoms was possible. The idea behind this technique is to reduce the exchange interaction constant J and to scale the geometrical dimensions (R and L) of the cylinder by means of a factor χ. Therefore, if we want to obtain the magnetic configuration of a cylinder whose geometrical size is given by R and L and its physical ferromagnetic exchange parameter is J, we only need to consider a much smaller system characterized by new parameters R', L', and J' which are related with the real ones as follows:

$$R' = \chi^\eta R, \quad L' = \chi^\eta L, \quad J' = \chi J, \qquad (10)$$

where $\chi < 1$. The scaling exponent determined in nanosized magnetic system has a nearly universal value of $\eta = 0.55$,

TABLE I. Geometry of simulated nanotubes.

Tube	N_r	N_c	N_T	L' (nm)	R' (nm)	L (nm)	R (nm)
NT1	20	72	1440	18.12	0.8	1361.6	60.2
NT2	20	36	720	9.06	0.8	680.8	60.2
NT3	20	27	540	6.79	0.8	510.6	60.2
NT4	20	18	360	4.53	0.8	340.4	60.2
NT5	30	27	810	6.79	1.2	510.6	90.3
NT6	30	18	540	4.53	1.2	340.4	90.3

different from the value of 0.5, which is the value found by using the continuum theory.[16,17] In spite of this apparent contradiction with continuum theory, we have to stress that this technique gives equivalent results as the micromagnetic simulation technique does, and therefore it can be viewed as an alternative method to simulate magnetic phases in nanoscopic systems. For a nanotube whose internal to external radii ratio is given by the geometrical factor β, we must scale both radii, R_i and R, and therefore its ratio $\beta = R_i/R = R_i'/R' = \beta'$ remains unchanged.

We use a scaling technique described above to study the magnetic properties of isolated nickel nanotubes. The physical parameters for this material are lattice parameter $a_0 = 0.356$ nm, magnetic moment per atom $\mu = 0.6\mu_B$, and a stiffness constant $A = 1.5 \times 10^{-11}$ J/m corresponding to an exchange constant $J = 4004.56$ kOe/μ_B. Nickel has an fcc cubic structure, with nearest-neighbor distance $a = a_0/\sqrt{2} = 0.252$ nm. We have simulated a single-wall nickel nanotube, which is generated by rolling up the compact surface [a square two-dimensional (2D) lattice] in such a way that the distance between all atoms is a after rolling up. This form of arranging the atoms in a tube geometry allows us to have the same number of atoms in every transversal ring of the nanotube. We have considered tubes where the nearest-neighbor number of every atom is 4 except in the two atomic rings at both extremes of the nanotube, where the number of nearest neighbors is 3.

The radius of a studied nanotube is limited by the following condition: the tube is composed of parallel rings separated by a distance a and the distance between neighbor atoms along a ring is also a. So the coordination numbers always satisfy the condition indicated above. We used a scaling factor of $\chi = 3.885 \times 10^{-4}$; therefore the real size of the nanotubes are given by Eq. (10), where R' and L' are the radius and length of the scaled (smaller) tube used in the simulation. Table I shows the geometry of the simulated nanotubes where N_r is the number of atoms in every ring, N_c is the number of parallel rings forming the nanotube, and N_T is the total number of atoms of the nanotube. Note that N_r is related to the scaled radius and the nearest-neighbor distance through $N_r = 2\pi R'/a$, whereas $N_c = L'/a$. We have arbitrarily chosen tubes with $N_r = 20$ and 30 to perform Monte Carlo simulations. We have used a equivalent temperature of $T = 1$ mK, therefore the magnetic configurations shown represent the magnetic equilibrium states.
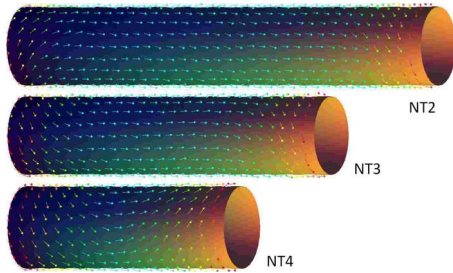
FIG. 2. (Color online) Equilibrium states at zero applied field for samples NT2, NT3, and NT4 (see Table I). The arrows represent the spins at each atomic site. We see clearly that these nanotubes show a symmetric mixed state.

IV. RESULTS AND DISCUSSION

In this section we show the results of magnetic equilibrium states for ferromagnetic nanotubes obtained by means of Monte Carlo simulations and theoretical calculations, as described in Secs. II and III. We begin with the Monte Carlo simulations, and then we provide a geometrical characterization of the mixed state based in our theoretical model. We also analyze the occurrence of different magnetic states by a comparison of their relative energies. This procedure allows us to obtain phase diagrams for magnetic nanotubes where the magnetic states are F (or uniform state), V, and M states. Finally, we apply a magnetic field to the mixed state and show how with our model we can study the nucleation of a vortex domain wall.

A. Mixed state

1. Monte Carlo simulations

In Fig. 2 we show the zero-field magnetic configuration of nanotubes NT2, NT3, and NT4 defined in Table I (NT1 is not shown due to their greater length). From this figure, we can see that the atoms at both tube ends tend to orient themselves perpendicular to the tube axis in a vortex configuration, whereas the atomic moments of the internal layers are oriented ferromagnetically parallel to the tube axis; i.e., the system shows a mixed magnetic state. Moreover we also observe that the ferromagnetic portion grows as the tube length grows and the vortex region remains approximately the same as the tube length grows. This is in agreement with our theoretical model where, provided that the tube length is greater than the size of the vortex region (d), the parameter d is independent of the length; it depends only on the tube cross section. We also observe no differences in the magnetization at both tube ends for all simulated cases. This is reasonable because asymmetries in the magnetization arise from imperfections of the nanotube geometry, surface defects, or differences in chemical composition as well, which we are not considering in this work.

Additionally our results show that the vortex region increases with the tube radius. For example, NT3 and NT5 (not shown here) have the same length and different radii, showing an increasing vortex region with the radius, and thus the fraction of ferromagnetic aligned magnetic moments dimin-
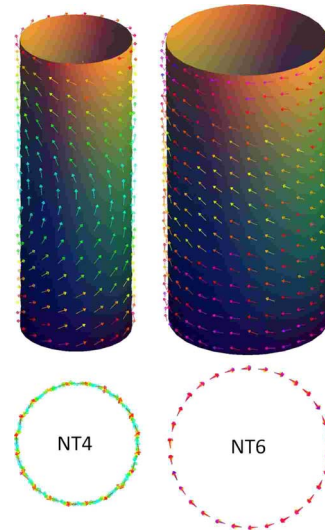

FIG. 3. (Color online) Equilibrium states at zero applied field for nanotubes NT4 and NT6 (see Table I), both with the same length. We see clearly that the smaller tube (NT4) shows a symmetric mixed state, whereas NT6 shows a vortex state. The lower panel depicts the top view, illustrating the null radial component of the magnetization in both tubes.

ishes with an increasing radius. This behavior is also observed from our analytical model, where we find that the size of the vortex region (d) increases with the radius as shown in Fig. 6.

We remark that all the simulated tubes show magnetic configurations without radial component of the magnetization vector. This can be seen in Fig. 3, where we show the equilibrium states for nanotubes NT4 and NT6 as indicated in Table I. We observe that for the nanotube with smallest length and largest radius (NT6), the ferromagnetic region has vanished and all magnetic moments deviate from the tube axis direction forming a vortex state. Thus we observe a transition from the mixed state to a vortex state, as a result of the increment in the tube radius. This point will be made clearer further on in this paper. In all cases, the magnetic equilibrium states of the nanotubes have the following property: the transition of the magnetization from one extreme to the other in a nanotube occurs by smooth changes in the axial and tangential components of the individual magnetic moments. We do not see any radial component of the magnetization because this would cause an increase in the total energy, principally as shape anisotropy (or dipolar energy). However, in a forthcoming work[22] about the dynamic motion of a vortex domain wall, it is shown that the magnetization can adopt a radial component, $M_\rho(z) = M_s \sin p \sin \Theta(z)$, which is created by the torque exerted by the applied field. Thus, the static magnetization is obtained with $p = 0$, and depending on the dynamic regime of the vortex wall motion, the angle p can increase.[22]

To be more specific, we have calculated the axial component of the magnetization [$M_z(z)$] in every tube cross section. We show the results in Fig. 4, where we can see that the deviation of the orientation from the z axis of the atomic spins is practically symmetric for all tubes. The small discrepancies are due to incomplete relaxation in the Monte
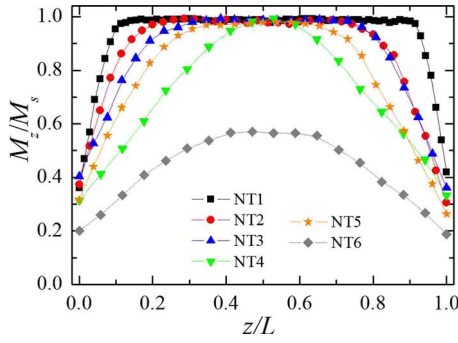
FIG. 4. (Color online) Axial magnetization (M_z) at zero applied field for simulated nanotubes NT1–NT6 (see Table I). Note that NT1–NT5 show a mixed state, whereas NT6 is most likely a vortex state although there remains some axial magnetization.

Carlo simulations. The number of points in each curve is equal to the number of rings of each nanotube. We can observe that nanotube NT4, corresponding to the smallest nanotube, only reach the value 1 in one point, indicating that this ring is the only one aligned ferromagnetically along the tube axis. On the other hand, the curve for NT6 depicts the result obtained for a wider nanotube of the same length that of NT4. Here we see that the z component of the normalized magnetization never reach the value 1, indicating that ferromagnetic portion has disappeared; indeed it is always less than 0.6. This result indicates that there is a transition from a mixed magnetic state to a vortex like state as the radius of the nanotube increases for a constant length.

An important and subtle issue to discuss is the sense of rotation of the vortex domains confined at the tube ends. In Figs. 2 and 3 we have represented the magnetic equilibrium state of the nanotubes, where we can observe differences in the sense of rotation of the magnetization at both extremes of the nanotubes. We can clearly appreciate that in some cases the senses of rotation of the magnetization are equal, whereas in other cases they are inverse. For instance the magnetization of NT3 (Fig. 2) has the same sense of rotation at both ends, whereas NT2 and NT4 have opposite senses of magnetization rotation. In general we have not found a sequential behavior of the rotation alignment of magnetization in both tube extremes as a function of their length or radius. Nonetheless, the micromagnetic simulations of Wang *et al.*[4] showed that the nearly zero-field equilibrium state is the so-called twisted bamboo phase which corresponds to the mixed state with an opposite circulation of the spins in the top and bottom extremes. This behavior was also observed by Lee *et al.*,[11] performing micromagnetic simulations on a Permalloy nanotube. The existence of a mixed state with opposite circulation of the magnetic moments at the tube ends remains to be fully acquainted for the case of single-wall magnetic nanotubes and will be reported elsewhere.

2. Analytical model

From the Monte Carlo simulations we see the basic phenomenology of the mixed state, but we cannot obtain a complete geometrical description of the problem. This can be investigated from our theoretical model described in Sec. II.
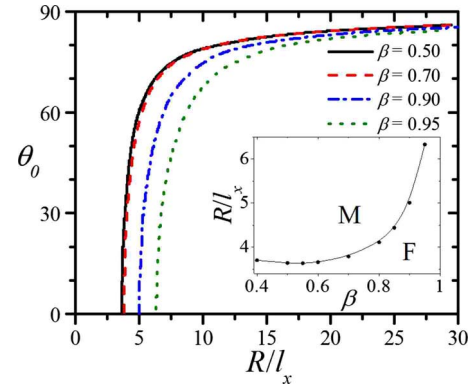

FIG. 5. (Color online) Variation in θ_0 with the radius (R) for different form factors β. The parameter θ_0 corresponds to the angle between the axis of the tube and the magnetization of the vortex domains at the extremes of the tube. These curves show the transition from ferromagnetic state ($\theta_0=0$) to the mixed state as R increases. The radius has been normalized to the exchange length l_x. The inset shows the critical radius at which $\theta_0=0$.

Performing a minimization procedure of the total energy of the mixed state, we can obtain the variation in the magnetization of this state with the geometrical parameters. The magnetization [see Eqs. (2) and (3)] is thus given by the parameters of the model, that is, the size of the vortex domains, d, and the angle θ_0, corresponding to the angle between the magnetization at the extremes of the tube, with the axis of the tube. Note that the axial component of the magnetization evaluated at the extremes is given by $M_z(z=0,L) = M_s \cos \theta_0$. We find that, provided that the tube length L is greater than $2d$, the size of the vortex domains is independent of L, and it only depends on β and R.

In Fig. 5 we show the angle θ_0 as a function of the tube radius normalized to the exchange length, $l_x=(2A/\mu_0 M_s^2)^{1/2}$, for $L=2000l_x$ and β varying from $\beta=0.50$ to 0.95 as indicated in the figure. We see that, for a special value of R, the angle θ_0 goes to zero, which means that the magnetization is fully oriented with the tube axis in a ferromagnetic state. Therefore we can define a critical radius $R^{F-M}(\beta)$ below which the magnetization is practically uniform along the axis, whereas above $R^{F-M}(\beta)$ the mixed state develops. The behavior of this critical radius as a function of β is shown in the inset of Fig. 5. We also observe that as R increases above $R^{F-M}(\beta)$, the angle θ_0 increases sharply until $\theta_0=70°$. Above 70° the increment of θ_0 with the radius is less abrupt and asymptotically tends to 90°.

In Fig. 6 we show the size of the vortex domains normalized to l_x as a function of R/l_x for $L=2000l_x$ and $\beta=0.50-0.95$. We see that d/l_x increases with R/l_x approximately as $(R/l_x)^{5/2}$. However, this increment is bounded by a natural limit, that is, the tube length L. Our calculations show that, as d reach the value $L/2$, which means that the vortex domains in both extremes joins in the middle of the tube ($z=L/2$), the vortex state has a lower energy than the mixed state. This can be seen in the phase diagrams of Sec. IV B as shown in Fig. 7. We also perform simple fits of the curves in Fig. 6, and then, depending on β, we can estimate the size of the vortex domains with the simple formula
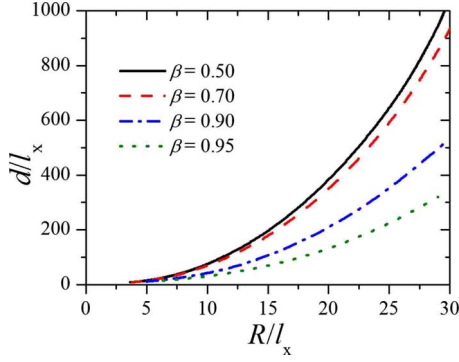
FIG. 6. (Color online) Variation in d with the radius (R) for different values of β. Here d corresponds to the size of the vortex domains confined at the extremes of the tube. The dimensions (d and R) have been normalized to the exchange length l_x.

$$d/l_x = 6 + (0.208 - 0.189\beta^{6.18})(R/l_x)^{5/2}. \quad (11)$$

We remark that our results are more suitable for nanotubes with $\beta \geq 0.5$ because we do not consider a possible dependence of the magnetization with the radial coordinate. As we have already characterized the mixed state, we are in position of determine the magnetic phase diagrams for ferromagnetic nanotubes, including the F, M, and V states.

Another interesting point to discuss is about the effect of other identical nanotubes in the equilibrium state. It has been show recently that, in the case of square arrays of magnetic nanodots in the vortex-core state, interdot dipolar interactions may change the equilibrium magnetization.[23] This dipolar induced change in the vortex-core size depends on the characteristics of the array (number of dots, interdot distance, and lattice) and also on the relative orientation of the vortex cores within the array: parallel cores shrink the core size in order to reduce the positive interaction energy, whereas cores oriented in opposite directions have a negative interaction energy and therefore the vortex core expands to lower the total energy.[23] More recently, Escrig *et al.*[24] investigated the magnetostatic coupling between two magnetic nanotubes with uniform magnetization. In the special case of two nano-
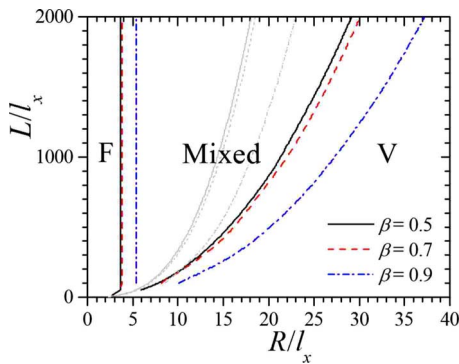

FIG. 7. (Color online) Magnetic phase diagrams for nanotubes with $\beta = 0.5$ (solid lines), $\beta = 0.7$ (dashed lines), and $\beta = 0.9$ (dash-dotted lines). The thin lines depicts the transition between F and V states, which splits into two lines corresponding to the transitions F-M and M-V.

tubes without vertical separation ($s=0$ in Ref. 24), starting from their equations, it can be easily shown that the interaction energy is positive if the magnetizations are parallel and negative if the magnetizations are antiparallel. This interaction energy must be further reduced if we consider the mixed states instead of the uniform states because the mixed states enclose the magnetic field in the tube ends reducing the stray field. However, the calculations of dipolar interactions between nanotubes in the mixed state have not been carried out yet. Nonetheless, we can expect changes in the mixed state as a result of interactions between nanotubes, that is, θ_0 and d must depend on the relative separation between both nanotubes. Once the interaction energy between two tubes in the mixed state it is calculated, one can extend the result to an array of nanotubes by using the methods presented by Laroze *et al.*[25]

B. Magnetic phase diagram

If we only consider the ferromagnetic and vortex states, it has been shown recently[9,10] that the phase diagram depends on the topological form factor β. In the limit of $L \gg R$, the critical line ($E^F = E^V$) that separates magnetic phases (F and V) follows the simple equation $L/l_x = \alpha(\beta)R^3/l_x^3$, where $\alpha(\beta)$ is a number of the order of 0.1 (see Figs. 3 and 4 in the paper of Escrig *et al.*[9]). Thus, to the left (right) of this curve we have $E^F < E^V$ ($E^F > E^V$).[9] However, if we evaluate the energy of the symmetric mixed state along the critical lines, we find that the mixed state has a lower energy than the two main states (F and V), over a wide range of geometrical parameters, and consequently the critical lines that separates phases F and V splits now in two lines, separating now phases F and M as well as M and V.

The energy of the ferromagnetic and vortex states was already calculated by Escrig *et al.*;[9] for instance see Eqs. (6) and (7) in that paper. We can also obtain the energy of the F state from the energy of the symmetric mixed state, in the limit $\theta_0 \to 0$ or $m_z(z) = 1$. The exchange energy of the F state is zero, as can be obtained in that limit from Eqs. (4) and (5). Furthermore, the dipolar energy [Eq. (6)] reduces to

$$E^F = \pi\mu_0 M_s^2 R^2 \int_0^\infty \frac{1 - e^{-qL}}{q^2}[J_1(qR) - \beta J_1(qR\beta)]^2 dq,$$

because from Eqs. (A5) and (A7) we find that $\Omega(q) = 2(1 - e^{-qL})/q$ and $\Gamma(q) = 0$, in agreement with Eq. (6) in the paper of Escrig *et al.*[9] Therefore, our model for the mixed state enables us to study the F state as well. On the other hand, the energy of the vortex state is given just by the exchange contribution,[9] in virtue of the flux-closure nature of the V state and reads $E^V = 2\pi LA \ln(1/\beta)$. With the above expressions for the energy of the three magnetic states, we can obtain the phase diagrams for different values of the form factor β. It is worth to mention that the mixed state requires a special treatment because a change in the tube radius induces changes in the mixed state, as we can see from Figs. 5 and 6 in Sec. IV A 2. Thus, by comparing the relative energies of the three states we can compute phase diagrams in the R/l_x-L/l_x plane, containing now three regions corresponding to the three equilibrium states, as shown in Fig. 7.

Here we show phase diagrams for magnetic nanotubes with $\beta=0.5$, 0.7, and 0.9, as indicated in Fig. 7. The thin lines depict the transition between F and V states for three indicated beta values and without considering mixed (M) states. Each one of these thin lines splits into two lines corresponding to the F-M and M-V transitions. We can clearly see that the mixed state is the equilibrium state in a wide region of the phase diagrams. The region of stability of the mixed state show a subtle behavior as we change the form factor β. An increment of β moves slightly the F-M transition line to the right. The M-V transition line also moves to the right but more than the F-M line. Finally, we see that thin-walled nanotubes (β close to 1), as the ones currently fabricated,[1–5] show mixed states with a wider region in the phase diagram.

We remark that our results are most suitable for tubes such that $L \geq 2d$ because our model for the mixed state does not consider configurations with touching vortex domains, and thus the phase diagrams cannot be accurately obtained for small values of L. For this reason, in the phase diagrams we focus on nanotubes with $L \gg R$. However, we do not perform the mathematical limit $L \gg R$ in our equations for the total energy; instead of it we search for solutions for d which are less than $L/2$.

C. Comparison between theory and simulation

A comparison between the analytical approach and the Monte Carlo simulations is appropriate. The principal difficulty in this direction is to give to our simulated nanotubes an accurate value of the form factor $\beta=R_i/R$. As mentioned earlier, we use the scaling technique performed on a 2D cylindrical shell, with a tube wall thickness $w'=R'-R_i'=R'(1-\beta')$. This quantity cannot be larger than the nearest-neighbor distance $a=0.2517$ nm; indeed it should be less than that because of the curved geometry but also larger or equal than the atomic radius of Ni which is $\langle r_a \rangle=0.135$ nm. On the other hand, w' has to be considered as a scaled dimension such as R' and L' and therefore, the real nanotube must have the same value of β, that is, $\beta'=\beta$. Thus, if we write $\beta=1-w'/R'$, with $0.135<w'<0.2517$ nm, the value of β must be constrained depending on the radius used in the simulations, $R'=aN_r/2\pi$. For NT1–NT4 the scaled radius correspond to $R'=0.8$ nm and therefore the value of β must be constrained to the interval $0.69<\beta<0.83$. Analogously, for NT5 and NT6 we have $R'=1.2$ nm, and therefore the value of β must satisfy $0.79<\beta<0.89$. A more accurate value of β can be found by comparing the simulation results with the theory. This can be done by calculating the behavior of the axial magnetization $m(z)$ along the tube axis.

The axial component of the magnetization is plotted in Fig. 8 along the nanotube axis normalized to L. The results of the Monte Carlo simulations are shown for NT1 (circles, lower panel) and NT2 (squares, upper panel), whereas the lines correspond to our model for different values of β. The considered nanotubes have a fixed radius and different lengths indicated in Table I. The curves with $\beta=0.8$ (solid lines) shows good agreement with the points obtained by means of Monte Carlo simulation although the curves with
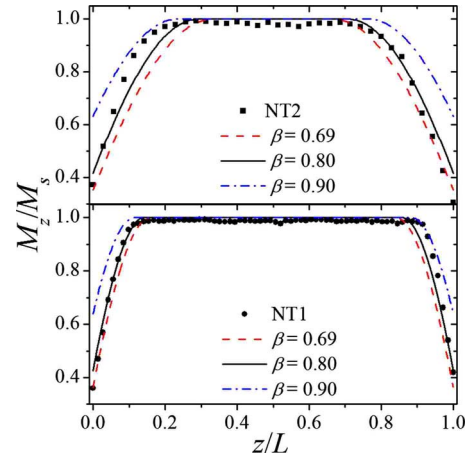

FIG. 8. (Color online) Axial magnetization along the tube axis normalized to L. The upper panel depicts the results for NT2 and the lower panel depicts that for NT1. Symbols represent the results of Monte Carlo simulations, and the lines are the theoretical results obtained for different values of β as indicated in the figure. We found agreement between theory and simulation for $\beta=0.69$ and 0.8.

$\beta=0.69$ (dashed lines) also present good agreement. However the curves with $\beta=0.9$ (dash-dotted lines) are less adequate to describe the Monte Carlo results. This is in agreement with the above discussions, where NT1–NT4 are better described by values of β which satisfy $0.69<\beta<0.83$, and for that reason $\beta=0.9$ does not represent the simulations.

D. Nucleation of a vortex domain wall

In this section we discuss the effect of an applied magnetic field ($\mathbf{H}=H\hat{z}$) on the nanotube magnetization. Similar to the Brown equations of magnetism,[18] our theory does not include dynamical effects, and therefore we can only focus our attention to a quasistatic applied fields or near to equilibrium processes. Under those assumptions we can use our energy calculations to gain some insight into the complicated magnetization process driven by an external field.

In Secs. IV A–IV C we have shown the magnetic structure of the mixed state. This state is modeled with two control parameters, θ_0 and d, which depending on the geometry assume different values, as can be seen in Figs. 5 and 6. We note that all the zero-field mixed states exhibit angles $\theta_0 <90°$, as can be seen in the curves of Fig. 5. This statement is also true in the overall mixed state region of the phase diagram (see Fig. 7). Thus, we can say that the magnetization of the mixed state is like an incomplete vortex wall localized at the extremes of the tube. These localized vortex walls can be set in motion with an applied field or maybe with thermal assistance or current-driven techniques through spin-torque effect. In the case that a magnetic field is the driven force, the reversal process must nucleate with an incomplete wall structure, as the mixed state, but now with $\theta_0 = \theta_0(H)$. Within this context, in the quasistatic limit, the nucleation field (H_n) can be calculated from $\theta_0(H_n)=0$ because it is the field at which the magnetization begin to change starting from the saturated state.[18] As the field is decreased from saturation
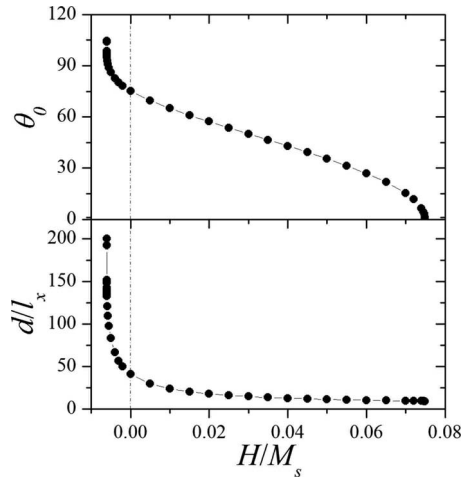
FIG. 9. External field dependence of the mixed state parameters, $\theta_0(H)$ and $d(H)$, for nanotubes with $\beta=0.9$, $R=10l_x$, and $L=5000l_x$. The behavior of the parameters near $H=-0.006M_s$ is a signature of a bistable reversal process. The nucleation field can be obtained as $\theta_0(H)=0$, which is near to $0.075M_s$.
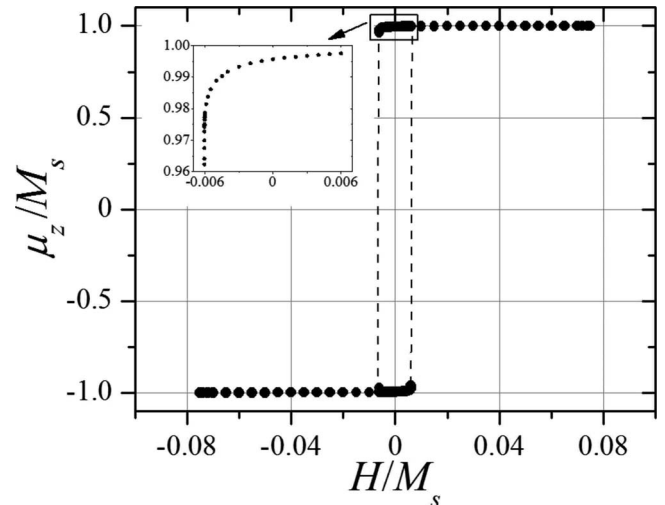

FIG. 10. Quasistatic hysteresis loop for nanotubes with $\beta=0.9$, $R=10l_x$, and $L=5000l_x$. The curve changes abruptly near $H=-0.006M_s$ which is a signature of a bistable reversal process. The inset shows a magnification of the region showed. The dashed lines are a guide for the eyes.

$[\theta_0(H)=0]$ to the nucleation field and beyond, the magnetization passes from a saturated state to a mixed state characterized by $\theta_0(H)>0$. We expect that a reduction in the magnetic field to values less than H_n shifts the angle $\theta_0=0$ to bigger values with an increment of the vortex wall size $d=d(H)$. This stage of the process can be considered as the beginning of the reversal mechanism and the nucleation field is precisely the field at which the original saturated state becomes unstable and any sort of change in the magnetization just starts.[18]

Our model allows us to analyze the application of a quasistatic field by including the Zeeman energy [Eq. (9)] in the exchange and dipolar contributions. In the case that the external field is not perfectly aligned with the z axis, the Zeeman energy can be obtained from Eq. (9) but H must be replaced by their component parallel to the z axis provided the angle between the external field and the magnetization be small enough. However, if this angle increases, we cannot describe with our model the nucleation of a vortex because the magnetization must deviate from the mixed state. Therefore, we focus our attention to an external field parallel (or almost parallel) to the z axis.

We have calculated numerically the parameters of the model which now depends on the field H. This can be seen in Fig. 9, where we show $\theta_0(H)$ and $d(H)$ for a nanotube with $\beta=0.9$, $R=10l_x$, and $L=5000l_x$. From this figure we can interpret the nucleation field H_n as the value at which $\theta_0(H_n)=0$, and the saturated state begin to lose their stability. On the other hand, note that as the field is decreased from saturation and becomes negative, the model's parameters grow quickly. Clearly, this is a signature of a bistable magnetization process, and we may consider the critical field ($H\approx-0.006M_s$) at which the model parameters grow with an infinite slope as a function of external field as a lower bound to the coercive field. More than frequently in the literature, the nucleation field is calculated in the so-called curling mode, which assumes an infinite sample.[18–21] In the curling mode there is no

dependence on the axial coordinate (z) and the first deviation of the magnetization occurs along the entire sample, not only in the tube ends, as expected.

A further comment is that the nucleation field is a theoretical concept and must be very difficult to measure. The reason of the above premise is that, at nucleation, the value of the net magnetization, μ_z, is very close to the saturation magnetization. From our model we can calculate μ_z by integrating M_z over the entire volume of the nanotube, that is, $\mu_z=(1/v)\int_v M_z(z)dv$, which after replacing M_z from Eqs. (2) and (3) reads

$$\mu_z(H) = M_s\left[1 - \frac{2d(H)}{L}\left(1 - \frac{\sin\theta_0(H)}{\theta_0(H)}\right)\right]. \qquad (12)$$

With this expression, we can calculate part of the hysteresis loop shown by the full symbols in Fig. 10. As our model allows us to describe the mixed state only with the vortex domains confined at the extremes of the tube, we cannot describe a domain wall within the nanotube and therefore we cannot construct a complete hysteresis loop; the dashed vertical lines are a guide for the eyes and do not represent any calculation. However, if desired, we could use the results of a previous work[13] for the exchange and dipolar energies of a vortex domain wall inside a nanotube and introduce a Zeeman term to obtain a complete "quasistatic" hysteresis loop. A complete study of the geometry dependence of the nucleation phenomena, as well as a complete description of the reversal process, will be published elsewhere. By the time, we focus our attention to the basic phenomenology of the nucleation problem.

In Fig. 10 we show $\mu_z(H)$ for a tube with $\beta=0.9$, $R=10l_x$, and $L=5000l_x$. Here, the inset shows a magnification of the curve, showing a signature of a bistable magnetization reversal process, because at the field $H\approx-0.006M_s$, the magnetization $\mu_z(H)$ changes abruptly.

We have briefly mentioned at the end of Sec. IV A the possible role of magnetostatic interactions between nanotubes in their equilibrium magnetization. To describe the effect of these interactions in the nucleation field and coercivity, it is necessary to add the full interaction energy in the array to the total self-energy of a number of nanotubes in the mixed state. Nonetheless, without performing these extensive calculations, we can expect that these interactions would reduce the nucleation field of any nanotube in the array because dipolar interactions prefer an antiparallel ordering between nanomagnets.[23–25]

We can conclude that the magnetization reversal process in nanotube occurs with the nucleation of vortex domains at the extremes of the tube. These domains can be set in motion with an applied field, and we have shown that the nucleation field cannot be used to evaluate the coercivity. Within our framework both fields are different by 1 order of magnitude; $H_n = 0.075 M_s$ and $H_c = -0.006 M_s$.

V. CONCLUSIONS

Equilibrium states of ferromagnetic nanotubes of Ni are well reproduced using Monte Carlo simulation with scaling, in agreement with previous micromagnetic simulations,[4,11,12] and present more general analytical model. Magnetic phase diagram as a function of tube length and radii shows that, at zero external field, the mixed state is more stable than pure ferromagnetic or vortex phases over a broad range of geometrical parameters. Quasistatic approximation allows us to estimate the nucleation field as well as coercivity under the application of an external field.

APPENDIX: MIXED STATE ENERGY

1. Exchange energy

The exchange energy in the continuum theory of ferromagnetism[18] is given by $E_x = A \int \Sigma (\nabla m_i)^2 dv$, and within our model [Eqs. (1) and (2)] we can write

$$E_x = 2\pi A \ln\frac{1}{\beta} \int_0^L \sin^2 \Theta(z)dz + \pi A R^2(1-\beta^2)\int_0^L \left(\frac{\partial \Theta}{\partial z}\right)^2 dz.$$

(A1)

By introducing our trial function, $\Theta(z)$ from Eq. (3) we obtain the exchange energy [Eq. (4)].

2. Dipolar energy

The dipolar contribution can be written as[18] $E_d = (\mu_0/2)\int \mathbf{M} \cdot \nabla U dv$, where U is the magnetostatic potential given by $U = \int \frac{\hat{\mathbf{n}}' \cdot \mathbf{M}(\mathbf{r}')}{4\pi |\mathbf{r}-\mathbf{r}'|} ds' - \int \frac{\nabla \cdot \mathbf{M}(\mathbf{r}')}{4\pi |\mathbf{r}-\mathbf{r}'|} dv'$. It can be shown that, for the mixed state we are describing, the potential depends only on the coordinates ρ and z and therefore $\partial U/\partial \phi = 0$. Moreover, the magnetization of the mixed state has no radial component, as we can see from our Monte Carlo simulations (for instance see Fig. 3), and therefore in cylindrical coordinates we have $\mathbf{M} \cdot \nabla U = M_z(z) \partial U/\partial z$ and the dipolar energy can be cast in the form

$$E_d = \pi \mu_0 \int_{R_i}^R \rho d\rho \int_0^L M_z(z) \frac{\partial U(\rho,z)}{\partial z} dz.$$

(A2)

In what follows, we calculate the surface and volumetric contributions to the magnetostatic potential, that is, $U = U_s + U_v$, and then the dipolar energy is given by $E_d = E_{ds} + E_{dv}$. To calculate the potential we use the following expansion:[26]

$$\frac{1}{|\mathbf{r}-\mathbf{r}'|} = \sum_{j=-\infty}^{\infty} e^{ij(\phi-\phi')} \int_0^{\infty} J_j(q\rho)J_j(q\rho')e^{-q|z-z'|}dq.$$

(A3)

a. Surface contribution

Using the above expansion, and after integration in coordinates ϕ' and ρ', the surface potential can be expressed as

$$U_s = \frac{1}{2}\int_0^{\infty} g(q)J_0(q\rho)[M_z(L)e^{-q(L-z)} - M_z(0)e^{-qz}]dq,$$

where we have defined $g(q) \equiv \int_{\beta R}^R J_0(q\rho)\rho d\rho = (R/q)[J_1(qR) - \beta J_1(qR\beta)]$. The energy associated with this potential can be expressed as

$$E_{ds} = \frac{\pi \mu_0 M_s^2}{2}\int_0^{\infty} g^2(q)q\Omega(q)dq,$$

(A4)

where

$$\Omega(q) = \int_0^L m_z(z)[m_z(L)e^{-q(L-z)} + m_z(0)e^{-qz}]dz.$$ (A5)

The function $\Omega(q)$ can be calculated easily by using our model to the mixed state [Eqs. (2) and (3)] but the result is long. In this paper we focus on the symmetric mixed state, that is, $\theta_L = \theta_0$ and $\lambda = d$, where the function $\Omega(q)$ can be further reduced to

$$\Omega(q) = \frac{2qd^2 \cos \theta_0}{(\theta_0^2 + q^2d^2)}\left\{\left(\frac{\theta_0}{qd}\right)^2 (e^{-qd} - e^{-q(L-d)})\right.$$
$$\left. + (1-e^{-qL})\cos \theta_0 + (1+e^{-qL})\frac{\theta_0}{qd}\sin \theta_0\right\}.$$

b. Volumetric contribution

It is a straightforward matter to show that $\nabla \cdot \mathbf{M} = \partial M_z/\partial z$. Using the expansion given in Eq. (A3) in the volumetric

potential, and after integration in coordinates ϕ' and ρ', the surface potential can be expressed as

$$U_v = -\frac{1}{2}\int_0^\infty dq J_0(q\rho)g(q)\int dz'\frac{\partial M_z(z')}{\partial z'}e^{-q|z-z'|}.$$

Clearly, $\partial U_v/\partial\phi = 0$, and after integration in the radial coordinate, the corresponding dipolar energy can be written as

$$E_{dv} = -\frac{\pi\mu_0 M_s^2}{2}\int_0^\infty g^2(q)\Gamma(q)dq, \qquad \text{(A6)}$$

where we have defined

$$\Gamma(q) \equiv \int_0^L m_z(z)\left(\frac{\partial}{\partial z}\int_0^L \frac{\partial m_z(z')}{\partial z'}e^{-q|z-z'|}dz'\right)dz. \quad \text{(A7)}$$

The integration of the above expression has to be done carefully because of the term with $e^{-q|z-z'|}$. Once the integration is performed, we obtain a long expression, which is further reduced in the symmetric mixed state; nevertheless the expression for $\Gamma(q)$ is still long. For this reason we do not write explicitly $\Gamma(q)$ in this appendix.

3. Zeeman energy

The energy of the mixed state associated with the applied magnetic field $\mathbf{H} = H\hat{\mathbf{z}}$ can be written as[18] E_Z $= -\mu_0 H M_s\int m_z(z)dv$, where H is the strength of the applied field, which can be positive or negative. By integrating in the radial and angular coordinates we can write

$$E_Z = -\mu_0 M_s H\pi R^2(1-\beta^2)\int_0^L \cos\Theta(z)dz,$$

and finally by using our model for the mixed state [Eq. (3)] we obtain the expression in Eq. (9).

4. Anisotropy contributions

The uniaxial anisotropy is given by[18] $E_u = -K_u\int m_z^2 dv$ and within our model for the mixed state, we can write

$$E_u = -\pi K_u(R^2 - a^2)\int_0^L \cos^2\Theta(z)dz,$$

with $\Theta(z)$ given by Eq. (3). After integration we obtain expression (7). On the other hand, the cubic anisotropy is usually given by[18] $E_c = K_c\int(m_x^2 m_y^2 + m_y^2 m_z^2 + m_z^2 m_x^2)dv$, and within our model [Eqs. (1) and (2)] we can write

$$E_c = \frac{\pi K_c}{8}R^2(1-\beta^2)\int_0^L \sin^2\Theta(z)[1 + 7\cos^2\Theta(z)]dz.$$

Finally, after integration we obtain expression (8).

*pedro.landeros@usm.cl

[1] Y. C. Sui, R. Skomski, K. D. Sorge, and D. J. Sellmyer, J. Appl. Phys. **95**, 7151 (2004); Y. C. Sui, R. Skomski, K. D. Sorge, and D. J. Sellmyer, Appl. Phys. Lett. **84**, 1525 (2004).

[2] K. Nielsch, F. J. Castaño, C. A. Ross, and R. Krishnan, J. Appl. Phys. **98**, 034318 (2005).

[3] K. Nielsch, F. J. Castaño, S. Matthias, W. Lee, and C. A. Ross, Adv. Eng. Mater. **7**, 217 (2005).

[4] Z. K. Wang, H. S. Lim, H. Y. Liu, S. C. Ng, M. H. Kuok, L. L. Tay, D. J. Lockwood, M. G. Cottam, K. L. Hobbs, P. R. Larson, J. C. Keay, G. D. Lian, and M. B. Johnson, Phys. Rev. Lett. **94**, 137208 (2005).

[5] M. Daub, M. Knez, U. Goesele and K. Nielsch, J. Appl. Phys. **101**, 09J111 (2007).

[6] S. J. Son, J. Reichel, B. He, M. Schuchman, and S. B. Lee, J. Am. Chem. Soc. **127**, 7316 (2005).

[7] D. L. Leslie-Pelecky, V. D. Labhasetwar, and R. H. Kraus, Jr., in *Advanced Magnetic Nanostructures*, edited by D. Sellmyer and R. Skomski (Springer, New York, NY, 2006), pp. 461–482.

[8] D. Lee, R. E. Cohen, and M. F. Rubner, Langmuir **23**, 123 (2007).

[9] J. Escrig, P. Landeros, D. Altbir, E. E. Vogel, and P. Vargas, J. Magn. Magn. Mater. **308**, 233 (2007).

[10] J. Escrig, P. Landeros, D. Altbir, and E. E. Vogel, J. Magn. Magn. Mater. **310**, 2448 (2007).

[11] J. Lee, D. Suess, T. Schrefl, K. H. Oh, and J. Fidler, J. Magn. Magn. Mater. **310**, 2445 (2007).

[12] A. P. Chen, N. A. Usov, J. M. Blanco, and J. Gonzalez, J. Magn. Magn. Mater. **316**, e317 (2007).

[13] P. Landeros, S. Allende, J. Escrig, E. Salcedo, D. Altbir, and E. E. Vogel, Appl. Phys. Lett. **90**, 102501 (2007).

[14] J. d'Albuquerque e Castro, D. Altbir, J. C. Retamal, and P. Vargas, Phys. Rev. Lett. **88**, 237202 (2002).

[15] P. Vargas, D. Altbir, and J. d'Albuquerque e Castro, Phys. Rev. B **73**, 092417 (2006).

[16] W. Zhang, R. Singh, N. Bray-Ali, and S. Haas, Phys. Rev. B **77**, 144428 (2008).

[17] P. Landeros, J. Escrig, D. Altbir, D. Laroze, J. d'Albuquerque e Castro, and P. Vargas, Phys. Rev. B **71**, 094435 (2005).

[18] A. Aharoni, *Introduction to the Theory of Ferromagnetism* (Clarendon, Oxford, 1996).

[19] Ching-Ray Chang, C. M. Lee, and Jyh-Shinn Yang, Phys. Rev. B **50**, 6461 (1994).

[20] R. Skomski, J. Phys.: Condens. Matter **15**, R841 (2003).

[21] J. Escrig, M. Daub, P. Landeros, K. Nielsch, and D. Altbir, Nanotechnology **18**, 445706 (2007).

[22] P. Landeros and Álvaro S. Núñez (unpublished).

[23] D. Altbir, J. Escrig, P. Landeros, F. S. Amaral, and M. Bahiana, Nanotechnology **18**, 485707 (2007).

[24] J. Escrig, S. Allende, D. Altbir, and M. Bahiana, Appl. Phys. Lett. **93**, 023101 (2008).

[25] D. Laroze, J. Escrig, P. Landeros, D. Altbir, M. Vázquez, and P. Vargas, Nanotechnology **18**, 415708 (2007).

[26] J. D. Jackson, *Classical Electrodynamics*, 2nd ed. (Wiley, New York, 1975).